Journal of Turbulence
Volume 6, No. 37, 2005

Taylor & Francis
Taylor & Francis Group

CVS and SCALES simulation of 3-D isotropic turbulence

DANIEL E. GOLDSTEIN*†, OLEG V. VASILYEV†
and NICHOLAS K.-R. KEVLAHAN‡

†Mechanical Engineering, University of Colorado at Boulder Boulder, CO, USA
‡Department of Mathematics and Statistics, McMaster University Hamilton, ON, Canada

In this work coherent vortex simulation (CVS) and stochastic coherent adaptive large eddy simulation (SCALES) simulations of decaying incompressible isotropic turbulence are compared to DNS and large eddy simulation (LES) results. Current LES relies on, at best, a zonally adapted filter width to reduce the computational cost of simulating complex turbulent flows. While there is an improvement over a uniform filter width, this approach has two limitations. First, it does not capture the high wave number components of the coherent vortices that make up the organized part of turbulent flows, thus losing essential physical information. Secondly, the flow is over-resolved in the regions between the coherent vortices, thus wasting computational resources. The SCALES approach addresses these shortcomings of LES by using a dynamic grid adaptation strategy that is able to resolve and track the most energetic coherent structures in a turbulent flow field. This corresponds to a dynamically adaptive local filter width. Unlike CVS, which we show is able to recover low order statistics with no subgrid scale (SGS) stress model, the higher compression used in SCALES necessitates that the effect of the unresolved SGS stresses must be modeled. These SGS stresses are approximated using a new dynamic eddy viscosity model based on Germano's classical dynamic procedure redefined in terms of two wavelet thresholding filters.

Keywords: Large Eddy Simulation; Stochastic Coherent Adaptive Large Eddy Simulation; Coherent Vortex Simulation; Turbulence; Wavelets; Wavelet Filtering

1. Introduction

Turbulence is characterized by energetic eddies that are localized in space and scale, yet most numerical methods for turbulent flow simulations do not take advantage of this localization. In this work we explore the possibility of making use of this localization by 'compressing' the turbulence problem such that a simulation with a subset of the total modes captures the dynamics of the most energetic eddies in the flow. A recent method for simulating turbulence called coherent vortex simulation (CVS), introduced by Farge *et al.* [1], uses a wavelet filter to dynamically resolve and 'track' the energetic coherent eddies or vortices in a turbulent flow. It has been shown that the resulting subgrid scale (SGS) field with CVS is near Gaussian white noise [2, 3], which results in practically no SGS dissipation. Therefore, a CVS simulation with no SGS model is shown to recover low-order and some high-order statistics [4]. It is important to note that there is still significant energy transfer between the resolved and SGS modes and vice versa, but the statistical average or net energy transfer is zero. If other higher order statistics are required, then a purely stochastic SGS stress model may be able to reproduce

*Corresponding author. E-mail: Daniel.E.Goldstein@colorado.edu

Journal of Turbulence
ISSN: 1468-5248 (online only)
http://www.tandf.co.uk/journals
DOI: 10.1080/14685240500460790

the effect of the SGSs more accurately. One of the challenges with the CVS method is how to determine on the fly during an actual simulation the 'ideal' wavelet compression, which results in a purely incoherent SGS field. Even if it can be found in a cost-effective manner, it is still likely that the associated adaptive grid will be too fine to be cost effective for simulating high Re number flows, since the computational cost of CVS falls between DNS and large eddy simulation (LES).

Recently a new methodology called stochastic coherent adaptive large eddy simulation (SCALES) [2] has been introduced that shares with CVS the ability to dynamically resolve and 'track' the most energetic part of the coherent eddies in a turbulent flow field, but with the higher computational efficiency associated with LES. With SCALES the maximum number of modes in the simulation are resolved, given there is a balance between computing resources and user defined acceptable simulation error. Thus, with SCALES the collocation grid dynamically adapts to the local flow in order to resolve the maximum portion of the coherent energetic eddies. With a field compression in the range of that used with typical LES applications, the SGS modes are no longer near Gaussian white noise, as in CVS, and so a SGS model is required. Yet at the same field compression as LES, the wavelet filter used with SCALES results in a significantly reduced level of total SGS dissipation [2]. This means that less of the flow needs to be modeled. In this work we apply the SCALES method to the problem of three-dimensional decaying incompressible isotropic turbulence.

An eddy viscosity type SGS model for SCALES is also investigated in this work. Since the wavelet threshold filter lacks a clearly defined global filter width, an alternative model scaling based on the non-dimensional wavelet threshold parameter ϵ is proposed. Results using a modified Smagorinsky [5] eddy viscosity SGS stress model, using both a constant model coefficient and a dynamic coefficient determined by a new dynamic procedure, are shown. This new dynamic procedure follows the derivation of Germano's [6–8] classical dynamic procedure. Test filtering is defined as a wavelet filter with threshold parameter equal to 2ϵ, and an explicit grid filter is used with a wavelet filter threshold parameter value of ϵ.

In this research, the CVS and SCALES methods have been implemented using a dynamically adaptive wavelet collocation (DAWC) method [9, 10]. The DAWC method is ideal for implementing CVS and SCALES as it combines the resolution of the energetic coherent modes in a turbulent flow with the simulation of their temporal evolution [2, 9–11]. The wavelet collocation method employs wavelet compression as an integral part of the solution such that the solution is obtained with the minimum number of grid points for a given accuracy. When the threshold is chosen simply to satisfy numerical accuracy (and SGSs are not modeled) we call this method wavelet based direct numerical simulation or WDNS [2, 11].

The rest of this paper is organized as follows. In section 2 the background theory and the results relevant to this work are presented. The LES method is introduced in section 2.1. Then the general properties of wavelets and, in particular, second-generation wavelets are introduced along with an introduction to wavelet threshold filtering in sections 2.2 and 2.3. The properties of wavelet compression and wavelet de-noising are then discussed in section 2.4. In section 3 a DAWC solver is introduced, which has been used to implement the CVS and SCALES methods. In section 4.1 the implementation of SCALES along with the introduction of a new dynamic SGS model is presented. Then in section 5 fully adaptive CVS and SCALES simulations of three-dimensional decaying incompressible isotropic turbulence based on the DAWC method are presented. Finally, the conclusions and the discussion of future work are presented in section 6.

2. Background

2.1 *Large eddy simulation*

The LES method is based on the premise that the large scales of a turbulent flow dominate mixing, heat transfer and other quantities of engineering interest, while the small scales are of interest only because of how they effect the large scales. The LES equations for incompressible flow, which describe the evolution of the large-scale eddies in the flow field, can be written as

$$\frac{\partial \overline{u_i}}{\partial x_i} = 0\,, \tag{1}$$

$$\frac{\partial \overline{u}_i}{\partial t} + \frac{\partial(\overline{u}_i\,\overline{u}_j)}{\partial x_j} = -\frac{1}{\rho}\frac{\partial \overline{p}}{\partial x_i} + \nu\frac{\partial^2 \overline{u}_i}{\partial x_j \partial x_j} - \frac{\partial \tau_{ij}}{\partial x_j}\,, \tag{2}$$

where

$$\tau_{ij} = \overline{u_i u_j} - \overline{u}_i\,\overline{u}_j \tag{3}$$

and u_i is the velocity field, ρ is density, ν is kinematic viscosity, p is pressure and $\overline{(\cdot)}$ represents spatial filtering. As a result of the filtering process, the unresolved quantity τ_{ij}, commonly referred to as the SGS stress, is introduced. Note that τ_{ij} is a function of the unfiltered velocity field u_i. In order to close (1) and (2) and realize the benefit of LES, a low-order model for the SGS stress, which is based on the resolved quantities, is needed. In practice τ_{ij} can be modeled either deterministically [12–14] or stochastically [15]. Most current LES is done using purely deterministic models.

In LES the filter is either explicit or it can be defined implicitly by the computational grid. Either way, LES uses a reduced computational grid that is capable of supporting (or representing) only a subset of the total number of active modes in the flow. Current state-of-the-art LES work uses non-uniformly stretched meshes or zonal grids [12, 16, 17] that are refined *a priori* to the geometry of the problem.

Current research efforts in LES are focused on finding improved SGS stress models for τ_{ij}. Currently, the most common SGS stress models used are of the eddy viscosity type [18]. These more advanced models are based on the simple one proposed by Smagorinsky [5]. In this type of model a linear eddy viscosity model is used to relate the SGS stress (τ_{ij}) to the filtered rate of strain (S_{ij}).

2.2 *General properties of wavelets*

Wavelets are basis functions that are localized in both physical space (due to their finite support) and wavenumber space (due to their vanishing moments), see e.g. figure 1. For comparison, the classical Fourier transform is based on functions (sines and cosines) that are well localized in wavenumber, but do not provide localization in physical space due to their global support. Because of this space/scale localization, the wavelet transform provides both spatial and scale (frequency) information, while the Fourier transform provides only frequency information.

A scalar field $f(\mathbf{x})$ can be represented in terms of wavelet basis functions as

$$f(\mathbf{x}) = \sum_{\mathbf{l}\in\mathcal{L}^0} c^0_{\mathbf{l}}\phi^0_{\mathbf{l}}(\mathbf{x}) + \sum_{j=0}^{+\infty}\sum_{\mu=1}^{2^n-1}\sum_{\mathbf{k}\in\mathcal{K}^{\mu,j}} d^{\mu,j}_{\mathbf{k}}\psi^{\mu,j}_{\mathbf{k}}(\mathbf{x}), \tag{4}$$

where $\phi^0_{\mathbf{k}}(\mathbf{x})$ and $\psi^{\mu,j}_{\mathbf{l}}$ are, respectively, n-dimensional scaling functions and wavelets of different families (μ) and levels of resolution (j). One may think of a wavelet decomposition

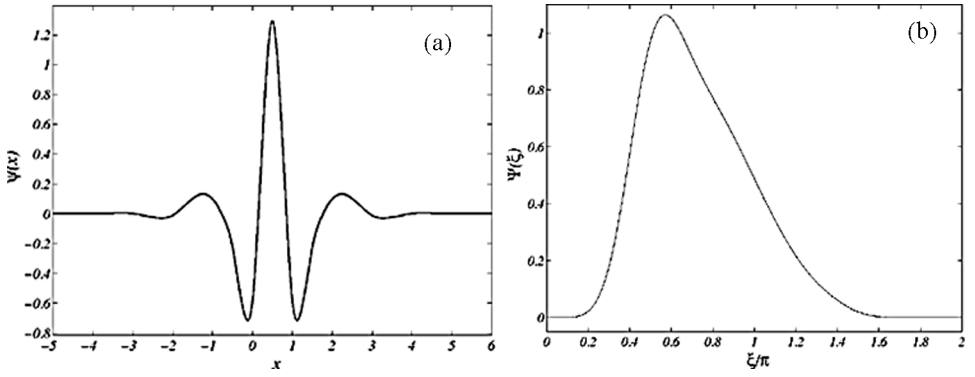

Figure 1. (a) Lifted interpolating wavelet ψ of order 6 (a) and (b) its Fourier transform $\Psi(\xi)$.

as a multilevel or multiresolution representation of a function, where each level of resolution j (except the coarsest one) consists of wavelets $\psi_{\mathbf{l}}^{j}$ or family of wavelets $\psi_{\mathbf{l}}^{\mu,j}$ having the same scale but located at different positions. Scaling function coefficients represent the averaged values of the field, while the wavelet coefficients represent the details of the field at different scales. The wavelet functions have a zero mean, while the scaling functions do not. Note that in n dimensions there are $2^n - 1$ distinctive n-dimensional wavelets [19]. Also note that because of the local support of both scaling functions and wavelets, there is a one-to-one correspondence between the location of each scaling function or wavelet with a grid point. As a result each scaling function coefficient $c_{\mathbf{l}}^{0}$ and each wavelet coefficient $d_{\mathbf{k}}^{\mu,j}$ is uniquely associated with a single grid point with the indices $\mathbf{l}$ and $\mathbf{k}$, respectively.

Traditionally, one-dimensional first-generation wavelets ψ_k^j are defined as translates and dilates of one basic wavelet ψ, i.e. $\psi_k^j(x) = \psi(2^j x - k)$. Second-generation wavelets [20, 21] are a generalization of first-generation wavelets that supply additional freedom to deal with arbitrary boundary conditions and irregular sampling intervals. Second-generation wavelets form a Riesz basis for $\mathbf{L}_2$ space, with the wavelets being local in both space and frequency and often having many vanishing polynomial moments, but without the translation and dilation invariance of their first-generation cousins. Despite the loss of these two fundamental properties of wavelet bases, second-generation wavelets retain many of the useful features of first-generation wavelets, including a fast $O(N)$ transform. The construction of second-generation wavelets is based on the lifting scheme, which is discussed in detail by Sweldens [20, 21].

For this study, we use a set of second-generation wavelets known in the literature as lifted interpolating wavelets [10, 20]. In particular, simulations with the DAWC solver are run using a lifted interpolating wavelet of order 6, which is shown in figure 1 along with its Fourier transform. For a more in-depth discussion on the construction of these wavelets, the reader may refer to the papers by Sweldens [20, 21] and Vasilyev and Bowman [10]. For a more general discussion on wavelets, we refer the reader to the books of Daubechies [19] and Mallat [22].

2.3 *Wavelet filters*

Wavelet filtering is performed in wavelet space using wavelet coefficient thresholding, which can be considered as a nonlinear filter that depends on each flow realization. The wavelet

thresholding filter is defined by

$$\overline{f}^{>\epsilon}(\mathbf{x}) = \sum_{\mathbf{l}\in\mathcal{L}^0} c_{\mathbf{l}}^0 \phi_{\mathbf{l}}^0(\mathbf{x}) + \sum_{j=0}^{+\infty}\sum_{\mu=1}^{2^n-1} \sum_{\substack{\mathbf{k}\in\mathcal{K}^{\mu,j} \\ |d_{\mathbf{k}}^{\mu,j}|>\epsilon||f||_{\mathrm{WTF}}}} d_{\mathbf{k}}^{\mu,j}\psi_{\mathbf{k}}^{\mu,j}(\mathbf{x})\,, \tag{5}$$

where $f(\mathbf{x})$ is a scalar field, $\epsilon > 0$ is the non-dimensional (relative) threshold parameter and $||\cdot||_{\mathrm{WTF}}$ is the wavelet threshold filtering (WTF) norm that provides the (absolute) dimensional scaling for filtered variable f. For instance, in the case of velocity, the (absolute) dimensional scaling can be specified as the L_2 norm ($||u_i||_{\mathrm{WTF}} = ||u_i||_2$) or the L_∞ norm ($||u_i||_{\mathrm{WTF}} = ||u_i||_\infty$). Note that once the WTF norm $||\cdot||_{\mathrm{WTF}}$ is specified, the wavelet thresholding filter (5) is uniquely defined by the non-dimensional threshold parameter ϵ.

The reconstruction error due to wavelet filtering with non-dimensional threshold parameter ϵ can be shown to be [9, 23]

$$||f(\mathbf{x}) - \overline{f}^{>\epsilon}(\mathbf{x})||_2 \le C\epsilon||f||_{\mathrm{WTF}} \tag{6}$$

for a sufficiently smooth function $f(\mathbf{x})$, where C is of order unity.

As will be shown later, when the wavelet threshold filter is applied to a system of evolution equations, each variable could be filtered according to equation (5). Once filtered, each variable could be integrated in time. However, this would lead to numerical complications due to the one-to-one correspondence between the location of a wavelet with a grid point. In particular, each variable would be solved on a different grid. In order to avoid this difficulty and make filtering of each term in the evolution equation easy, in the present study the coupled wavelet thresholding strategy is used. The mask of significant wavelet coefficients is constructed for each variable according to the thresholding criteria of equation (5). The union of these masks will result in the *global* thresholding mask, which is used for each dependent variable and each term in the equation. Note that in some applications, additional variables, such as vorticity or strain rate, can be used for the construction of the *global* mask. Once this *global* mask is constructed, one can view the wavelet filtering as local low-pass filtering, where the high frequencies are removed according to the *global* mask. The effective wavelet filter width depends on the choice of WTF norm, the spatial distribution of the variables used for defining the coupled wavelet filter mask and is a function of the non-dimensional threshold parameter ϵ. Such interpretation of WTF highlights the similarity between the SCALES and the classical LES approaches. However, the wavelet thresholding filter is drastically different from the LES filters, primarily because it changes in time following the evolution of the solution, which in turn results in an adaptive computational grid that tracks in physical space the areas of locally significant energy of all variables used for the grid adaptation. However, it is important to note that, unlike the Fourier modes, there is no one-to-one correspondence between the wave number and the wavelet level. Instead, each wavelet level represents a region of wave numbers. Figure 2 shows the energy spectra of the modes associated with 6 wavelet scales or levels along with the full energy spectra of a turbulent field, obtained from a 256^3 DNS simulation of forced isotropic turbulence [24] with $\mathrm{Re}_\lambda = 168$. Note that this turbulent field will hereafter be referred to as F_{256}. This figure highlights the fact that each wavelet scale has energy in a region of wave numbers and that these regions overlap.

2.4 *Wavelet compression and wavelet de-noising*

The major strength of wavelet filtering decomposition (5) is the ability to compress signals. For functions that contain isolated small scales on a large-scale background, most wavelet coefficients are small and thus we can retain good approximation even after discarding a large

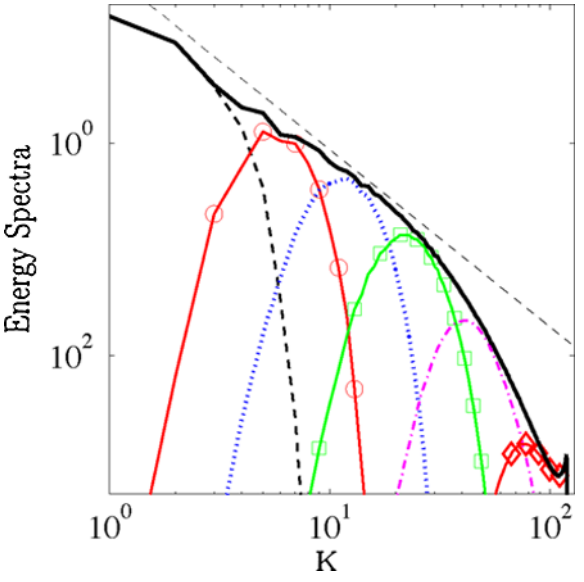

Figure 2. Energy spectra of turbulent velocity field F_{256}: (▬▬), contained in wavelet levels. Level 1: (- - - -), Level 2: (—○—), Level 3: (· · · · · · · ·), Level 4: (—□—), Level 5: (— · —), Level 6: (—◇—)

number of wavelets with small coefficients. Intuitively, the coefficient $d_{\mathbf{l}}^{\mu,j}$ will be small unless $u(\mathbf{x})$ has variation on the scale of j in the immediate vicinity of wavelet $\psi_{\mathbf{l}}^{\mu,j}(\mathbf{x})$.

Another important property of wavelet analysis used in this work is the ability of the wavelets to de-noise signals. The wavelet de-noising procedure, also called wavelet-shrinkage, was introduced by Donoho [25, 26] and is based on the orthogonal wavelet decompositions. It can be described as follows: given a function that consists of a smooth function with superimposed noise, one performs a forward wavelet transform and sets to zero 'noisy' wavelet coefficients (i.e., those wavelet coefficients whose modulus squared is less than the noise variance σ^2), otherwise the wavelet coefficient is kept. This procedure is known as hard thresholding. Donoho [25] demonstrated that hard thresholding is optimal for de-noising signals in the presence of Gaussian white noise. In the CVS method discussed in this work the 'noise' is actually the SGS modes.

3. Dynamically adaptive wavelet collocation method

A key component in the implementation of the SCALES method is the development of a DAWC [9–11, 27] solver. This solver is ideally suited to the simulation of turbulence since wavelets adapt the numerical resolution naturally to the localized turbulent structures that exist at all wave numbers in a fully developed turbulence. The wavelet collocation method takes advantage of the fact that wavelets are localized in both space and scale, and as a result, functions with localized regions of sharp transition are well compressed using wavelet decomposition. The adaptation is achieved by retaining only those wavelets whose coefficients satisfy the thresholding criteria of equation (5). Thus, high-resolution computations are carried out only in those regions where sharp transitions occur. With this adaptation strategy, a solution is obtained on a near optimal grid that 'tracks' the coherent vortices in the field, i.e., far fewer grid points are needed for wavelets than for conventional finite-difference, finite-element

or spectral methods [28]. By varying the threshold parameter ϵ, this method can be used to implement any of the wavelet-based methods discussed above, namely WDNS, CVS or SCALES. The DAWC collocation algorithm has already been successfully applied to the solution of thermo-acoustic wave propagation problems [27], combustion problems [9, 10], fluid–structure interaction problems [11], viscoelastic flows [29, 30] and the compaction phenomenon in a poro-viscoelastic matrix [31].

Let us briefly outline the main features of the numerical method. Details can be found in Refs. [9, 10]. In the wavelet collocation method, there is a one-to-one correspondence between grid points and wavelets. This makes the calculation of nonlinear terms simple and allows the grid to adapt automatically to the solution at each time step by adding or removing wavelets. Very briefly, at each time step we take the wavelet transform of the solution and apply the *global* thresholding mask to remove wavelets, which do not satisfy the thresholding criteria of equation (5) for all of the adaptation variables. To account for the evolution of the solution over one time step, the computational grid needs to be extended to include grid points associated with wavelets whose coefficients are, or can possibly become, significant during the time integration step [32]. To do this we add grid points that are adjacent in both position and scale to each significant wavelet coefficient. While the cost of this added adjacent zone is significant at low compression ratios, it becomes much less so at higher compression ratios. This diminishing cost of the adjacent zone with increased compression will be the case for any numerical problem that has inherent local structures that dominate the field being simulated. Figure 3 shows the compression ratio vs. the wavelet filter threshold parameter ϵ for a wavelet collocation grid adapted to a DNS field of isotropic turbulence ($\mathrm{Re}_\lambda = 168$) with and without an adjacent zone. For this *a priori* test, the coupled wavelet filter was applied on the basis of the wavelet thresholding of the velocity components using L_∞ WTF norm. We can see clearly that the added overhead of the adjacent zone becomes insignificant for compression ratios over 98%. This is the case because in turbulent flows, like the one considered, the flow is dominated by localized energetic coherent vortices. This trend will also hold for other common flows such as flow fields involving vortices due to fluid–structure interaction or shocks in compressible flow fields. Since each wavelet corresponds to a single grid point, this procedure allows the

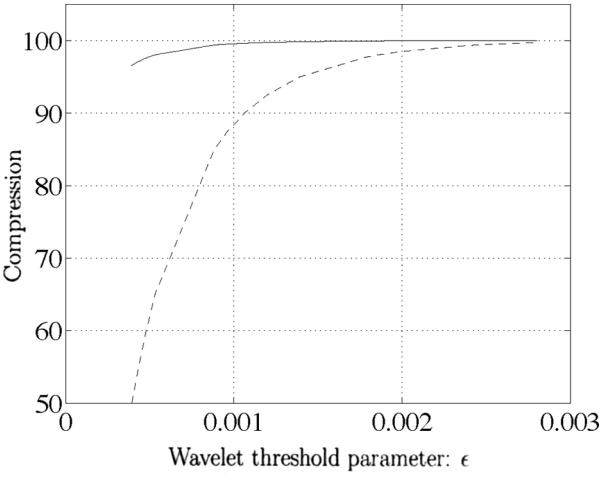

Figure 3. Field compression vs. relative wavelet threshold parameter ϵ, using velocity wavelet filtering, without adjacent zone (——-) and with adjacent zone (- - - - - - - -) for field F_{256}. It can be seen that as ϵ increases, the loss in compression due to the adjacent zone becomes less significant. The (absolute) dimensional scaling $||u_i||_{\mathrm{WTF}} = ||u_i||_\infty$ was used in the wavelet filtering for this *a priori* test.

grid to automatically follow the evolution of the solution in position and scale. We use second-generation wavelets [21], which allow the order of the wavelet (and hence of the numerical method) to be varied easily. The method has a computational complexity $O(N)$, where N is the number of wavelets retained in the calculation (i.e., the union of those wavelets with coefficients greater than $\epsilon||f_i||_{\mathrm{WTF}}$ for all adaptation variables, plus nearest neighbors).

In summary, the DAWC method is an adaptive, variable-order method for solving partial differential equations with localized structures that change their location and scale in space and time. Because the computational grid automatically adapts to the solution (in position and scale), we do not have to know *a priori* where the regions of high gradients or structures exist. In related work the DAWC method has been combined with the Brinkman penalization method [11, 33] to define solid structures in the domain for the simulation of complex geometry flows.

4. SCALES implementation

The SCALES method is based on the premise that the most energetic coherent vortices (or structures) of a turbulent flow dominate mixing, heat transfer and other quantities of engineering interest, while the smaller incoherent background is of interest only because of how it affects the energetic coherent vortices [2]. The SCALES equations for incompressible flow, which describe the evolution of the most energetic coherent vortices in the flow field, can be written as

$$\frac{\partial \overline{u_i}^{>\epsilon}}{\partial x_i} = 0, \tag{7}$$

$$\frac{\partial \overline{u_i}^{>\epsilon}}{\partial t} + \frac{\partial (\overline{u_i}^{>\epsilon}\,\overline{u_j}^{>\epsilon})}{\partial x_j} = -\frac{1}{\rho}\frac{\partial \overline{p}^{>\epsilon}}{\partial x_i} + \nu\frac{\partial^2 \overline{u_i}^{>\epsilon}}{\partial x_j \partial x_j} - \frac{\partial \overline{\tau_{ij}}^{>\epsilon}}{\partial x_j}, \tag{8}$$

where

$$\overline{\tau_{ij}}^{>\epsilon} = \overline{u_i u_j}^{>\epsilon} - \overline{u_i}^{>\epsilon}\,\overline{u_j}^{>\epsilon} \tag{9}$$

and u_i is the velocity field, ρ is density, ν is kinematic viscosity, p is pressure and $\overline{(\cdot)}^{>\epsilon}$ represents spatial filtering with a coupled wavelet thresholding filter. As a result of the filtering process the unresolved quantity $\overline{\tau_{ij}}^{>\epsilon}$, commonly referred to as the subgrid scale (SGS) stress, is introduced. Note that $\overline{\tau_{ij}}^{>\epsilon}$ is a function of the unfiltered velocity field u_i. In order to close (7) and (8) and realize the benefits of SCALES, a low-order model for the SGS stress based on the resolved quantities is needed. Also note that analogous to LES with non-uniform filter width [34–36] there is a commutation error between wavelet filtering and derivative operators, the effect of which is not considered in this paper. We note though that a significant number of points below the thresholding level, $\epsilon||u_i||_{\mathrm{WTF}}$, are retained due to the adjacent zone and reconstruction check procedures [9, 10, 37] in the regions of the energetic vortices, and these result in a significant reduction of the commutation error.

4.1 *SCALES SGS modeling*

The standard Smagorinsky [5] eddy viscosity SGS stress model defines an eddy viscosity that is proportional to the filter width and the characteristic filtered rate of strain. In the case of the coupled nonlinear wavelet thresholding filter used in SCALES, the filter width is implicitly defined by the non-dimensional wavelet threshold parameter ϵ. Therefore in SCALES, ϵ is

used to properly scale the eddy viscosity:

$$\nu_T = C_\epsilon \ell^2 \epsilon^\alpha ||\overline{S}^{>\epsilon}||, \tag{10}$$

where C_ϵ is non-dimensional model coefficient, ℓ is the global characteristic length scale and

$$\overline{S_{ij}}^{>\epsilon} = \frac{1}{2}\left(\frac{\partial \overline{u_i}^{>\epsilon}}{\partial x_j} + \frac{\partial \overline{u_j}^{>\epsilon}}{\partial x_i}\right) \tag{11}$$

is the strain rate of the resolved scales. Note that the model units do not depend on α simply because ϵ is non-dimensional. We will show in section 4.2 that appropriate scaling is obtained with $\alpha = 2$. The new linear eddy viscosity model is then used to define a model for the SGS stress (9):

$$\overline{\tau_{ij}^M}^{>\epsilon} \equiv -2\nu_T \overline{S_{ij}}^{>\epsilon}, \tag{12}$$

where ν_T is the turbulent eddy viscosity.

In this work the global characteristic length scale ℓ is introduced to obtain the proper units for the eddy viscosity ν_T. In addition, the length scale is assumed to be independent of the filter threshold parameter ϵ. With these two assumptions, the exact definition of ℓ does not need to be specified, since the whole group $C_\epsilon \ell^2 \epsilon^\alpha$ is determined by the dynamic procedure. ℓ^2 can be interpreted as an averaged characteristic length scale that is absorbed into the dynamic procedure. Currently we are working on the extension of the model that uses a local characteristic length scale ℓ, interpreted as the local characteristic vortical length scale implicitly defined by the wavelet thresholding filter.

The new Germano dynamic formulation for the model coefficient C_ϵ is thus based on the wavelet filter threshold parameter ϵ. For the dynamic procedure, the grid filter is defined as $\overline{(\cdot)}^{>\epsilon}$ and the 'test' filter is defined as $\overline{(\cdot)}^{>2\epsilon}$. The adjacent zone is excluded in both cases to obtain the proper model scaling. The dynamic procedure is then based on the original SGS stress equation (9) and an alternative SGS stress

$$\overline{T_{ij}}^{>2\epsilon} = \overline{\overline{u_i u_j}^{>\epsilon}}^{>2\epsilon} - \overline{\overline{u_i}^{>\epsilon}}^{>2\epsilon}\,\overline{\overline{u_j}^{>\epsilon}}^{>2\epsilon}, \tag{13}$$

which would result from applying the wavelet thresholding test filter ($\overline{(\cdot)}^{>2\epsilon}$) to (7)–(9). Note that the wavelet filter is a projection operator and therefore by definition

$$\overline{(\cdot)}^{>\epsilon_C} \equiv \overline{\overline{(\cdot)}^{>\epsilon_A}}^{>\epsilon_B}, \tag{14}$$

where $\epsilon_C = \max(\epsilon_A, \epsilon_B)$. Filtering (9) at the test filter level and subtracting it from (13) results in the modified Germano's identity [6]:

$$\overline{T_{ij}}^{>2\epsilon} - \overline{\overline{\tau_{ij}}^{>\epsilon}}^{>2\epsilon} = \overline{\overline{u_i}^{>\epsilon}\overline{u_j}^{>\epsilon}}^{>2\epsilon} - \overline{\overline{u_i}^{>\epsilon}}^{>2\epsilon}\,\overline{\overline{u_j}^{>\epsilon}}^{>2\epsilon}. \tag{15}$$

Then, substituting the modeled SGS stresses at the two filter levels into (15) gives

$$\begin{aligned}\overline{T_{ij}}^{>2\epsilon} - \overline{\overline{\tau_{ij}}^{>\epsilon}}^{>2\epsilon} &\approx \overline{T_{ij}^M}^{>2\epsilon} - \overline{\overline{\tau_{ij}^M}^{>\epsilon}}^{>2\epsilon} \\ &= 2C_\epsilon \ell^2 (2\epsilon)^2 ||\overline{S}^{>2\epsilon}||\overline{S_{ij}}^{>2\epsilon} - 2C_\epsilon \ell^2 \epsilon^2 \overline{||\overline{S}^{>\epsilon}||\overline{S_{ij}}^{>\epsilon}}^{>2\epsilon}.\end{aligned} \tag{16}$$

Following Lilly's [8] notation we define L_{ij} and M_{ij} as follows:

$$L_{ij} = \overline{\overline{u_i}^{>\epsilon}\overline{u_j}^{>\epsilon}}^{>2\epsilon} - \overline{\overline{u_i}^{>\epsilon}}^{>2\epsilon}\,\overline{\overline{u_j}^{>\epsilon}}^{>2\epsilon}, \tag{17}$$

$$M_{ij}\ell^2\epsilon^2 = 2\overline{||\overline{S}^{>\epsilon}||\overline{S_{ij}}^{>\epsilon}}^{>2\epsilon} - 8||\overline{S}^{>2\epsilon}||\overline{S_{ij}}^{>2\epsilon}, \tag{18}$$

where L_{ij} is the wavelet-filtered analog of the Leonard stress. This results in an overdetermined system of equations that can be used to find $C_\epsilon \ell^2 \epsilon^2$

$$C_\epsilon \ell^2 \epsilon^2 M_{ij} = L_{ij} \ . \tag{19}$$

Following Lilly's [8] least square solution to this system, we obtain the following expression for the local Smagorinsky model coefficient:

$$C_\epsilon \ell^2 \epsilon^2 = \frac{L_{ij} M_{ij}}{M_{ij} M_{ij}} \ . \tag{20}$$

With this model formulation $C_\epsilon \ell^2 \epsilon^2$ can be locally positive or negative, which allows for local backscatter of energy to resolved scales. In practice it has been found that locally negative values of $C_\epsilon \ell^2 \epsilon^2$ cause numerical instabilities in SCALES, as in LES, so we average over homogeneous directions:

$$C_\epsilon \ell^2 \epsilon^2 = \frac{\langle L_{ij} M_{ij} \rangle}{\langle M_{ij} M_{ij} \rangle} \ , \tag{21}$$

where $\langle \cdot \rangle$ denotes volume averaging.

4.2 *Model scaling*

If we assume that, with an appropriate value for α, the eddy viscosity model (10)–(12) provides the right dissipation it is easy to show

$$2C_\epsilon \ell^2 \epsilon^\alpha = -\frac{\left\langle \tau_{ij} \overline{S_{ij}}^{>\epsilon} \right\rangle}{\left\langle ||\overline{S}^{>\epsilon}|| \overline{S_{ij}}^{>\epsilon} \overline{S_{ij}}^{>\epsilon} \right\rangle}, \tag{22}$$

where α is the scaling law and ℓ is taken to be constant over the domain. The correct scaling is determined from *a priori* testing, using the isotropic turbulence field F_{256}. In figure 4 the scaling of $-\langle \tau_{ij} \overline{S_{ij}}^{>\epsilon} \rangle / \langle ||\overline{S}^{>\epsilon}|| \overline{S_{ij}}^{>\epsilon} \overline{S_{ij}}^{>\epsilon} \rangle$ is shown over a range of ϵ that corresponds to a field compression over the range of 78.5–99.95%. The slope of the curve in log–log axis determines the appropriate ϵ scaling. As can be seen, the quantity $\langle \tau_{ij} \overline{S_{ij}}^{>\epsilon} \rangle / \langle ||\overline{S}^{>\epsilon}|| \overline{S_{ij}}^{>\epsilon} \overline{S_{ij}}^{>\epsilon} \rangle$ scales roughly as ϵ^2 for a wide range of compressions. However, some deviation from this scaling is observed above 99.4% compression. Based on this *a priori* test of the scaling, the new dynamic Smagorinsky-type eddy viscosity model (10) has been implemented. The results of simulations with this new SGS model are presented in section 5 below.

5. Results

To validate the CVS and the SCALES methods, numerical simulations of decaying incompressible isotropic turbulence are considered. For this work the incompressible Navier–Stokes equations (7)–(9) are solved with the DAWC solver. Continuity (9) is enforced using a multistep pressure correction time integration method [38]. An adaptive wavelet collocation multilevel elliptic solver [37] is used in solving the Poisson equation for pressure at each time step.

Results of decaying incompressible isotropic turbulence with initial $\mathrm{Re}_\lambda = 72$ are presented. The simulations were initialized with a 128^3 forced isotropic turbulence DNS field from a de-aliased pseudo-spectral code. The DNS simulation was run using a resolution of 128^3 and had an initial eddy-turnover time of approximately 0.1. The spectral content of the initial DNS field is fully resolved by doubling the non-adaptive field resolution to 256^3 in the simulations.

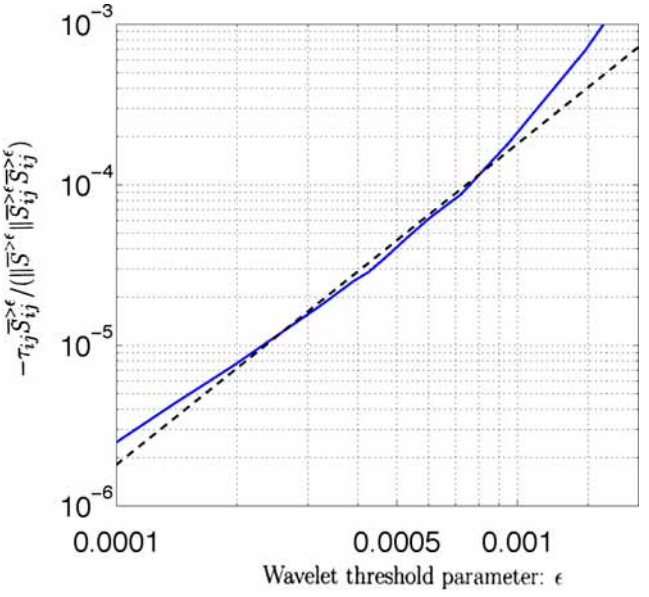

Figure 4. $\tau_{ij}\overline{S_{ij}}^{>\epsilon}/(||\overline{S}^{>\epsilon}||\overline{S_{ij}}^{>\epsilon}\overline{S_{ij}}^{>\epsilon})$ vs. relative wavelet threshold parameter ϵ, using velocity wavelet filtering, without adjacent zone (————) for field F_{256}. The dashed line is ϵ^2. The L_∞ WTF norm was used for this *a priori* test. This range of ϵ corresponds to a field compression over the range of 78.5–99.95%. It can be seen that $\tau_{ij}\overline{S_{ij}}^{>\epsilon}/(||\overline{S}^{>\epsilon}||\overline{S_{ij}}^{>\epsilon}\overline{S_{ij}}^{>\epsilon})$ scales roughly as ϵ^2. The scaling begins to deviate at $\epsilon = 0.001$, which corresponds to 99.4% compression.

This is required because the DAWC solver uses finite differences, which cannot resolve the full spectral content of the spectral DNS field at the original resolution. The results are compared to a full DNS performed with the de-aliased pseudo-spectral code used to generate the initial DNS field.

In running these simulations it has been determined that a more 'complete' adjacent zone than the partial adjacent zone described in section 3 is needed to limit the numerical and aliasing error at the high field compression used in SCALES. In the original adjacent zone, neighboring points on the level above, the current level and the level below are added around each active wavelet. From this point on, we will refer to this as a partial adjacent zone. This partial adjacent zone is used in the CVS simulations presented in section 5.1. For the high compression SCALES simulations presented in section 5.2, we have defined a complete adjacent zone that, in addition to the immediate neighbors, adds the diagonal neighbors.

For all SCALES and CVS results in this work, the L_2 WTF norm was used in the coupled wavelet filtering for grid adaptation based on the velocity field and for grid and test filtering in the model. Tests were also run using L_∞ WTF norm, but it was determined that this was considerably noisier due to temporal intermittency.

5.1 *CVS*

CVS simulations of decaying incompressible isotropic turbulence have been performed with no SGS stress model to validate the method's ability to dynamically resolve and track the coherent energetic eddies in a turbulent flow. A partial adjacent zone has been used for these simulations. In figures 5–8, the results of CVS and SCALES with no SGS stress model, for brevity called $\text{SCALES}_{\text{no-mdl}}$, are compared to DNS. It can be seen in figure 5 that the

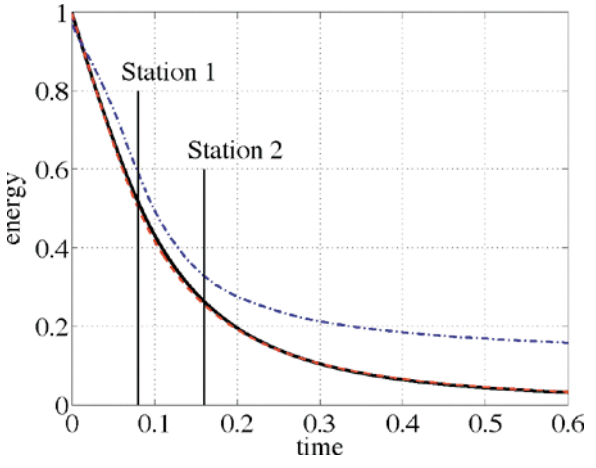

Figure 5. Energy decay for Case$_{Re_\lambda=72}$ with partial adjacent zone for CVS with no SGS model (– – – –), SCALES with no SGS model (— – —) and for comparison DNS (———). Large eddy turn over time for the initial DNS field is approximately 0.1. Two stations are shown at which energy spectra will be presented.

energy decay for CVS is nearly identical to the DNS. The SCALES$_{no-mdl}$ case is seen to be under dissipative. Figure 6 shows the field compression for CVS and SCALES$_{no-mdl}$. The compression stated is always with respect to the maximum field resolution, which in this case is 256^3. It can be seen that CVS is able to reproduce the DNS energy decay with a compression ranging from a minimum of 98.2–99.8% as the flow becomes laminar. This means that a maximum of 1.8% of the total modes are resolved in the CVS simulation. This variation of field compression over the course of the simulation reflects the decreasing amount of small-scale structures as the turbulence intensity decreases. In these simulations ϵ is set to 0.15 for CVS and 0.5 for SCALES$_{no-mdl}$. The value of ϵ for CVS was chosen iteratively to find the maximum value for which the energy decay over the simulation period closely matched that obtained with the DNS. For comparison CVS simulations (not shown) with $Re_\lambda = 48$ have been run. For these $Re_\lambda = 48$ simulations, 6% of the modes were required to match the DNS energy decay. This trend of compression scaling between $Re_\lambda = 48$ and

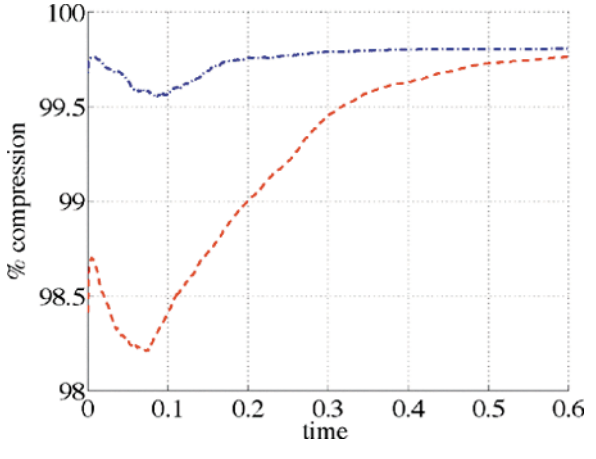

Figure 6. Field compression for Case$_{Re_\lambda=72}$ with partial adjacent zone for CVS with no SGS model (– – – –) and SCALES with no SGS model (— – —).

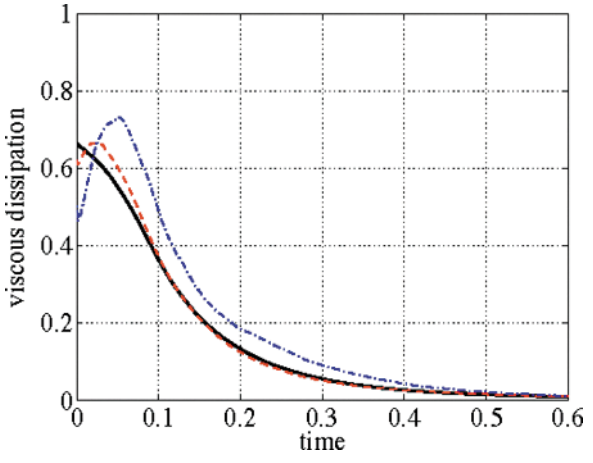

Figure 7. Total resolved viscous dissipation ($-\nu S_{ij} S_{ij}$) for Case$_{\mathrm{Re}_\lambda=72}$ with partial adjacent zone for CVS with no SGS model (– – – –), SCALES with no SGS model (— – —) and for comparison DNS (———).

72 is believed to be indicative of the expected scaling of CVS compression with Reynolds number. More data points are needed at higher Reynolds number to validate this possible level of scaling. In this CVS simulation the skewness of the first velocity derivative is maintained to within 10% of the DNS value, which reflects the fact that the CVS is resolving most of the DNS energy dissipation. In figure 7 we see that, after an initial period where the small scales are being recovered from the initial field projection, the total viscous dissipation of CVS closely matches the DNS. This confirms the hypothesis that with CVS the total SGS dissipation is minimal. This also indicates that the CVS is capturing the coherent structures, allowing the CVS simulation to at least partially resolve the energy cascade over all active wavenumbers. In figure 8 the energy spectra for CVS, SCALES$_{\mathrm{no-mdl}}$ and DNS are shown for two stations. The first station is at $t = 0.08$ and the second station is at $t = 0.16$. These stations are also shown on figure 5. The CVS spectra closely matches that of the unfiltered DNS at both

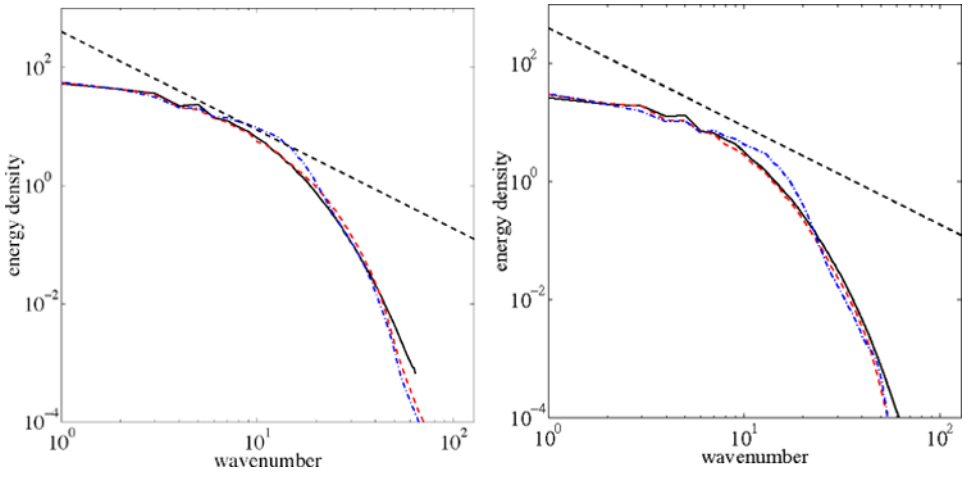

Figure 8. Energy spectra for Case$_{\mathrm{Re}_\lambda=72}$ with partial adjacent zone for CVS with no SGS model (– – – –), SCALES with no SGS model (— – —) and for comparison DNS (———), at time $t = 0.08$ (left) and 0.16 (right). A $k^{-5/3}$ straight dashed black line is shown to indicate the inertial range.

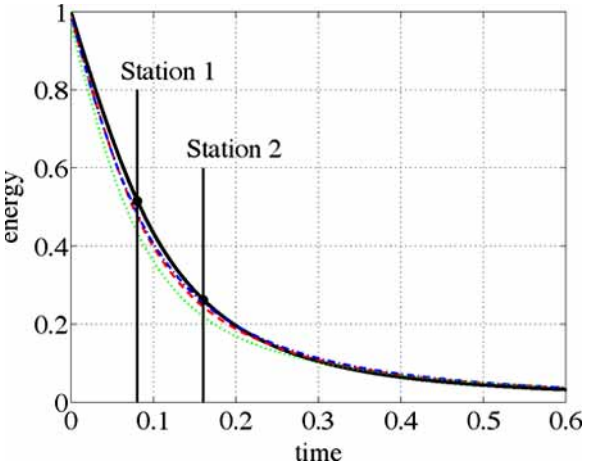

Figure 9. Energy decay for $\text{Case}_{\text{Re}_\lambda=72}$ with complete adjacent zone for SCALES with dynamic SGS model (– – – –), SCALES with SGS model coefficient $C_\epsilon \ell^2 \epsilon^2 = 0.0001$ (— – —), LES with dynamic SGS model (·····) and for comparison DNS (———). Large eddy turn over time for the initial DNS field is approximately 0.1. Two stations are shown at which energy spectra will be presented.

stations. Notice how with CVS the full energy spectra is closely resolved over the full spectral range. The spectra for the $\text{SCALES}_{\text{no-mdl}}$ case is seen to build up energy due to lack of SGS dissipation.

5.2 *SCALES constant coefficient and dynamic SGS stress model*

SCALES simulations have been performed with the constant coefficient Smagorinsky eddy viscosity model, equation (10), and the new dynamic Smagorinsky eddy viscosity SGS stress model described in section 4.1. The model coefficient ($C_\epsilon \ell^2 \epsilon^2 = 0.0001$) for the $\text{SCALES}_{\text{Cs}}$ case was chosen to best match the DNS results. For the $\text{SCALES}_{\text{dyn}}$ case the volume averaged

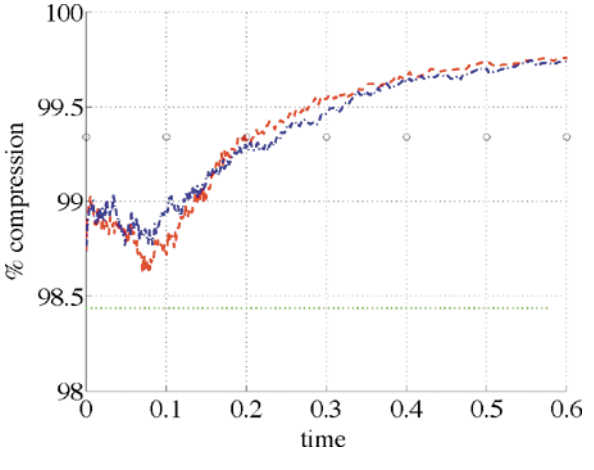

Figure 10. Field compression for $\text{Case}_{\text{Re}_\lambda=72}$ with complete adjacent zone for SCALES with dynamic SGS model (– – – –), SCALES with SGS model coefficient $C_\epsilon \ell^2 \epsilon^2 = 0.0001$ (— – —) and LES with dynamic SGS model (·····). The complete interpretation of the LES compression based on the 3/2 rule is shown as small circles.

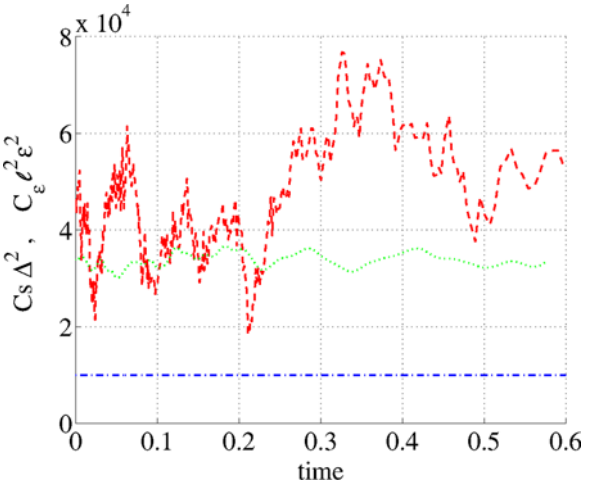

Figure 11. Dynamic SGS model coefficient for $\text{Case}_{\text{Re}_\lambda=72}$ with complete adjacent zone for SCALES with dynamic SGS model, $C_\epsilon \ell^2 \epsilon^2$ (– – – –), SCALES with SGS model coefficient $C_\epsilon \ell^2 \epsilon^2 = 0.0001$ (— – —) and LES with a classical dynamic SGS model, $C_s \Delta^2$(·····).

version of the dynamic model coefficient is used (21). These SCALES simulations, hereafter for brevity called $\text{SCALES}_{\text{Cs}}$ and $\text{SCALES}_{\text{dyn}}$ respectively, are compared to DNS and LES simulations. For both $\text{SCALES}_{\text{Cs}}$ and $\text{SCALES}_{\text{dyn}}$, cases ϵ is set to 0.5. The LES simulation is performed in the DAWC solver with a regular 64^3 grid, using the classical dynamic Smagorinsky model. The simulation is de-aliased by performing a wavelet transform on the velocity field and zeroing the highest level wavelet coefficients, thus resulting in a 32^3 solution at the end of the time step. This is more expensive than the 3/2 rule used in pseudo-spectral simulations. Figure 9 shows that the resolved kinetic energy decay for the $\text{SCALES}_{\text{dyn}}$ and $\text{SCALES}_{\text{Cs}}$ cases closely matches that of the DNS. The LES deviates slightly more from the DNS. Note that because of the similarity of the $\text{SCALES}_{\text{dyn}}$ and $\text{SCALES}_{\text{Cs}}$ results, the lines are difficult to distinguish. The $\text{SCALES}_{\text{dyn}}$ and $\text{SCALES}_{\text{Cs}}$ results lines are those just below the DNS line and above the LES line. In figure 10 the compression for the $\text{SCALES}_{\text{dyn}}$,

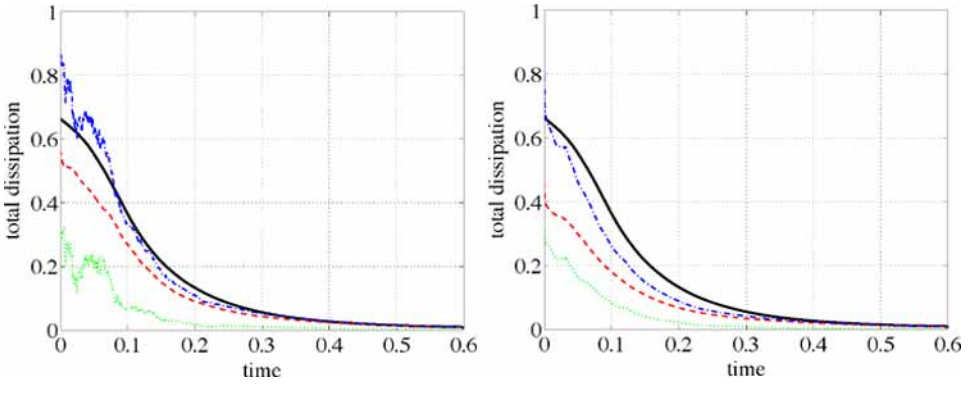

Figure 12. Resolved and SGS dissipation for (left) SCALES with the dynamic model and (right) SCALES with SGS model coefficient $C_\epsilon \ell^2 \epsilon^2 = 0.0001$, for $\text{Case}_{\text{Re}_\lambda=72}$ with complete adjacent zone. On both plots the DNS viscous dissipation is shown (———) with the viscous dissipation (– – – –), SGS dissipation (·····) and viscous + SGS dissipation (— – —).

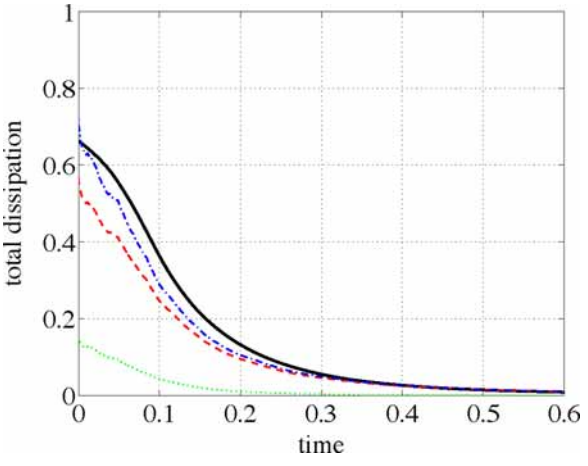

Figure 13. Resolved and SGS dissipation for LES with the dynamic model for $\text{Case}_{\text{Re}_\lambda=72}$. The DNS viscous dissipation is shown (———) with the viscous dissipation (– – – –), SGS dissipation (·····) and viscous + SGS dissipation (— – —).

$\text{SCALES}_{\text{Cs}}$ and LES cases are shown. If we consider the overhead of the modes used for de-aliasing, the LES may be considered to have a compression of 98.44%. The modes used for de-aliasing in LES can be considered as analogous to the adjacent zone in SCALES, so for a realistic comparison we can consider that if the LES was performed in a spectral code, using the 3/2 rule for de-aliasing, the effective compression would be 99.34% (shown in figure 10 as small circles). This is 0.35% higher than the initial compression of the $\text{SCALES}_{\text{dyn}}$ simulation. However, as the SCALES simulations progress the adaptive compression increases, surpassing that of the LES. Therefore, it can be said that the $\text{SCALES}_{\text{dyn}}$ and $\text{SCALES}_{\text{Cs}}$ simulations were able to capture the energy decay with a compression similar to a de-aliased LES simulation. In figure 11 we see that the dynamic model coefficient for $\text{SCALES}_{\text{dyn}}$ is more variable in comparison to the LES case. We conjecture that this variability could reflect

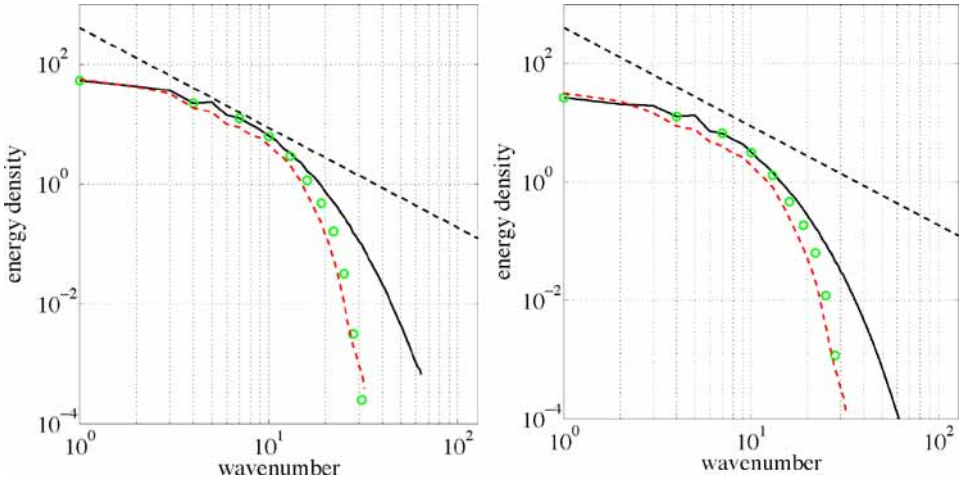

Figure 14. Energy spectra for $\text{Case}_{\text{Re}_\lambda=72}$ with complete adjacent zone for LES with dynamic SGS model (– – – –) at time $t = 0.08$ (left) and 0.16 (right). For comparison the DNS (———) and filtered DNS (○) are shown. A $k^{-5/3}$ straight dashed black line is shown to indicate the inertial range.

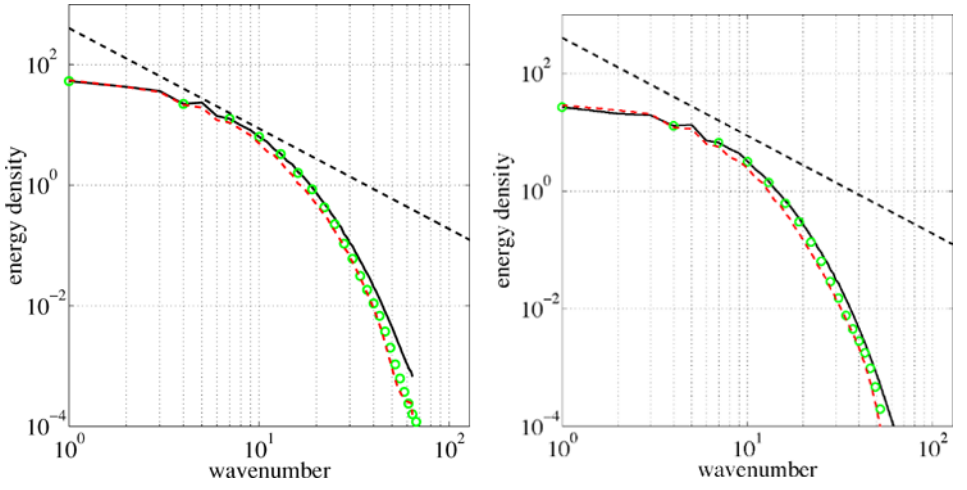

Figure 15. Energy spectra for $\text{Case}_{\text{Re}_\lambda=72}$ with complete adjacent zone for SCALES with SGS model coefficient $C_\epsilon \ell^2 \epsilon^2 = 0.0001$ (– – – –) at time $t = 0.08$ (left) and 0.16 (right). For comparison the DNS (———) and filtered DNS (○) are shown. A $k^{-5/3}$ straight dashed black line is shown to indicate the inertial range.

the sensitivity of the $\text{SCALES}_{\text{dyn}}$ model to actual localized events, such as energetic coherent vortex interactions that cause local high resolved stresses. These events must be included to properly characterize the instantaneous SGS dissipation. Further research is needed to understand this phenomenon. In figures 12 and 13 the viscous and SGS dissipations are presented for $\text{SCALES}_{\text{dyn}}$, $\text{SCALES}_{\text{Cs}}$ and LES. The variability of the $\text{SCALES}_{\text{dyn}}$ model coefficient is reflected in the $\text{SCALES}_{\text{dyn}}$ SGS dissipation. In figures 14–16 the energy spectra for the two stations shown in figure 9 are compared to the appropriately filtered DNS for the $\text{SCALES}_{\text{dyn}}$, $\text{SCALES}_{\text{Cs}}$ and LES cases. In comparison to LES, the DNS is filtered using a spherical Fourier cutoff filter equivalent to the maximum wave number resolved in the LES calculation. In the case of the SCALES simulations the appropriate DNS filtering for comparison is a wavelet

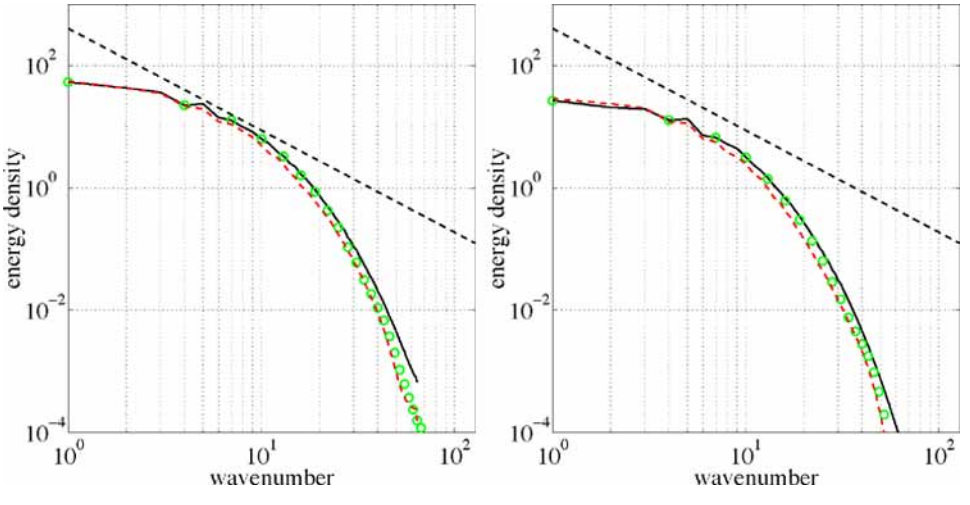

Figure 16. Energy spectra for $\text{Case}_{\text{Re}_\lambda=72}$ with complete adjacent zone for SCALES with dynamic SGS model (– – – –) at time $t = 0.08$ (left) and 0.16 (right). For comparison the DNS (———) and filtered DNS (○) are shown. A $k^{-5/3}$ straight dashed black line is shown to indicate the inertial range.

thresholding filter with equivalent threshold parameter to that used in the SCALES simulations. It can be seen that while there is reasonable agreement for the LES case (figure 14), the agreement with the filtered DNS is significantly improved for the $\text{SCALES}_{\text{Cs}}$ (figure 15) and $\text{SCALES}_{\text{dyn}}$ cases (figure 16). At both stations, in the dissipative range, the $\text{SCALES}_{\text{Cs}}$ and $\text{SCALES}_{\text{dyn}}$ simulations reproduce more of the high wave number energy. At the second station it can be seen in the inertial range that the LES has dissipated slightly more then the $\text{SCALES}_{\text{Cs}}$ and $\text{SCALES}_{\text{dyn}}$ cases. It is of particular interest to note that the wavelet filtered DNS in figures 15 and 16 are closer to the full DNS spectra over the full spectral range. Thus, the ability of SCALES to closely recover the filtered DNS results in a solution that has a spectral content close to the original unfiltered DNS solution over the whole DNS spectral range.

6. Conclusions

In this work dynamic simulation results of decaying incompressible isotropic turbulence using a new methodology for simulating turbulent flows called SCALES [2] are presented. This method combines the strengths of CVS and LES. The SCALES methodology uses the idea of WTF of the turbulent field as in CVS [1], but in SCALES the wavelet filter threshold is increased such that only the most energetic part of the coherent vortices is simulated in the resolved field. This enables the method to attain high rates of compression and makes it appropriate for simulating high Reynolds number flow. Indeed, the high compression achieved with SCALES should be even more advantageous at high Reynolds numbers due to turbulence intermittency.

In this research, the CVS and SCALES methods have been implemented using a DAWC method [9, 10]. The DAWC method is ideal for WDNS, CVS and SCALES since it combines the resolution of the energetic coherent modes in a turbulent flow with the simulation of their temporal evolution [2, 9–11]. A new dynamic SGS stress modeling procedure has been introduced based on a variation of the classical Smagorinsky [5] model. In our wavelet filtered version of the model, the scaling of the eddy viscosity is based on ϵ^2 (where ϵ is the wavelet filtering threshold parameter) instead of the standard scaling $\overline{\Delta}^2$ (where Δ is the filter width). In this new model a global characteristic length scale is introduced, which does not need to be specified, since it is absorbed by the dynamic procedure. The use of a local characteristic length scale, implicitly defined by the wavelet thresholding filter, is the subject of ongoing research. *A priori* results using forced incompressible isotropic turbulence have been presented that show this scaling holds for a wide range of compressions. The new dynamic procedure is similar in spirit to the classical dynamic procedure of Germano's [6–8], except that a new scaling law, based on ϵ^2, is used.

Dynamic simulations of SCALES, CVS and LES of decaying incompressible isotropic turbulence with a Taylor Reynolds number of $\text{Re}_\lambda = 72$ have been compared to DNS results to validate the SCALES and CVS methods with the DAWC solver. It has been shown that the adaptive CVS simulations closely match the DNS energy decay with only 1.8% of the modes of the DNS. We anticipate that CVS will work for even higher compression at higher Reynolds number flows due to increased flow intermittency. Dynamic SCALES simulations with the new dynamic modeling procedure use a complete adjacent zone (including diagonal neighbors) to cope with high compressions. The SCALES results with the dynamic model are shown to reproduce the DNS energy decay with only 1% of the DNS modes. The moderate increase in compression over the CVS calculations was due to the increased adjacent zone used in the SCALES calculations. It is anticipated that in higher Reynolds number simulations the cost of this complete adjacent zone will become minimal due to higher compression and

increased intermittency of the coherent structures. These SCALES results are also compared to fully de-aliased LES calculations. The SCALES results moderately outperformed those of the LES at a similar field compression.

While it is expected that for Reynolds numbers higher than the ones considered in this study the reduced SGS dissipation and increased incoherency of the SCALES SGS stress will provide significant improvement in SGS model accuracy, this is not the greatest potential benefit of the SCALES method. Flows of engineering and scientific interest occur in complex domains with large temporal and spatial variation in turbulence intensity. Therefore, an efficient simulation method must be capable of dynamically adapting the resolution over a wide range of local Reynolds numbers, often including large regions of laminar flow. A good example of this is flow over an aircraft, where the flow ranges from nearly laminar in the far field to intensely turbulent near the control surfaces. Another area of great potential benefit is in the simulation of fluid–structure interaction. In this case there is often no way to know in advance what sort of computational grid is needed since the structure can move or deform in unpredictable ways. Therefore, the trade-off between costly grid refinement over regions of potentially high turbulence intensity versus the loss of simulation accuracy must be balanced. With the SCALES methodology the collocation grid automatically adapts to the local flow at each time step in order to maintain a specified *a priori* accuracy. The required accuracy is specified with the wavelet filter threshold parameter (ϵ). For these reasons even if the SCALES methodology can do no better than match the cost of classical LES methods in unit test problems, like the ones conducted in this work, there is strong evidence to believe that SCALES will outperform classical LES in many complex real world flows at high Reynolds numbers. However, to realize the benefits of SCALES in such highly non-homogenous flows in complex geometries, a local SGS model and efficient data structures are required.

Acknowledgments

This work was supported by the Department of Energy (DOE) under Grant No. DE-FG02-05ER25667, the National Aeronautics and Space Administration (NASA) under grant No. NAG-1-02116, the National Science Foundation (NSF) under grants No. EAR-0327269 and ACI-0242457, and the Natural Sciences and Engineering Research Council of Canada. The authors would also like to thank the Shared Hierarchical Academic Research Computing Network and the Minnesota Supercomputing Institute for providing computational resources.

References

[1] Farge, M., Schneider, K. and Kevlahan, N., 1999, Non-Gaussianity and coherent vortex simulation for two-dimensional turbulence using an adaptive orthogonal wavelet basis. *Physics of Fluids*, **11**(8), 2187–2201.

[2] Goldstein, D.E. and Vasilyev. O.V., 2004, Stochastic coherent adaptive large eddy simulation method. *Physics of Fluids*, **16**(7), 2497–2513.

[3] Farge, M., Pellegrino, G. and Schneider, K., 2001, Coherent vortex extraction in 3d turbulent flows using orthogonal wavelets. *Physical Review Letters*, **87**(5).

[4] Schneider, K., Farge, M., Pellegrino, G. and Rogers, M., 2005, Coherent vortex simulation of three-dimensional turbulent mixing layers using orthogonal wavelets. *Journal of Fluid Mechanics*, **534**, 39–66.

[5] Smagorinsky, J.S., 1963, General circulation experiments with the primitive equations. *Monthly Weather Review*, **91**, 99–164.

[6] Germano, M., Piomelli, U., Moin, P. and Cabot. W.H., 1991, A dynamic subgrid-scale eddy viscosity model. *Physics of Fluids A*, **3**(7), 1760–1765.

[7] Germano, M., 1992, Turbulence: the filtering approach. *Journal of Fluid Mechanics*, **238**, 325–336.

[8] Lilly, D.K., 1992, A proposed modification to the Germano subgrid-scale closure model. *Physics of Fluid*, **3**, 633–635.

[9] Vasilyev, O.V., 2003, Solving multi-dimensional evolution problems with localized structures using second generation wavelets. (Special issue on High-resolution methods in Computational Fluid Dynamics). *International Journal Computing Fluid Dynamic*, **17**(2), 151–168.

[10] Vasilyev, O.V. and Bowman, C., 2000, Second generation wavelet collocation method for the solution of partial differential equations. *Journal of Computatinal Physics*, **165**, 660–693.
[11] Kevlahan, N.K.-R. and Vasilyev, O.V., 2005, An adaptive wavelet collocation method for fluid-structure interaction at high Reynolds numbers. *SIAM Journal of Scientific Computing*, **26**(6), 1894–1915.
[12] Moin, P., 2002, Advances in large eddy simulation methodology of complex flows. *International Journal of Heat and Fluid Flow*, **23**, 710–720.
[13] Lesieur, M. and Metais, O., 1996, New trends in large-eddy simulations of turbulence. *Annual Review of Fluid Mechanics*, **28**, 45–82.
[14] Meneveau, C. and Katz, J., 2000, Scale-invarience and turbulence models for large-eddy simulation. *Annual Review of Fluid Mechanics*, **32**, 1–32.
[15] Chasnov, J.R., 1991, Simulation of the Kolmogorov inertial subrange using an improved subgrid model. *Physics of Fluids A*, **3**, 188–200.
[16] Piomelli, U., 1999, Large-eddy simulation: achievements and challenges. *Progress in Aerospace Sciences*, **35**, 335–362.
[17] Kravchenko, A.G., Moin, P. and Moser, R., 1996, Zonal embedded grids for numerical simulations of wall-bounded turbulent flows. *Journal of Computational Physics*, **127**, 412–423.
[18] Pope, S.B., *Turbulent Flows* (Cambridge: Cambridge University Press.) 2000.
[19] Daubechies, I., *Ten Lectures on Wavelets*, Number 61 in CBMS-NSF Series in Applied Mathematics Philadelphia: SIAM. 1992.
[20] Sweldens, W., 1996, The lifting scheme: A custom-design construction of biorthogonal wavelets. *Applied and Computational Harmonic Analysis*, **3**(2), 186–200.
[21] Sweldens, W., 1998 The lifting scheme: A construction of second generation wavelets. *SIAM Journal of Mathematical Analysis*, **29**(2), 511–546.
[22] Mallat, S.G., *A Wavelet Tour of Signal Processing* (Paris: Academic Press.) 1999.
[23] Donoho, D.L. Interpolating wavelet transforms, Technical Report 408. Department of Statistics, Stanford University, 1992.
[24] Jimenez, J., Wray, A., Saffman, P. and Rogallo. R., 1993, The structure of intense vorticity in isotropic turbulence. *Journal of Fluid Mechanics*, **225**, 65–90.
[25] Donoho, D., 1993, Unconditional bases are optimal bases for data compression and for statistical estimation. *Applied and Computational Harmonic Analysis*, **1**, 100–115.
[26] Donoho, D.L. 1994, De-noising by soft-thresholding. *IEEE Transactions of Information Theory*, **41**(3), 613–627.
[27] Vasilyev, O.V. and Paolucci, S., 1997, A fast adaptive wavelet collocation algorithm for multi-dimensional PDEs. *Journal of Computational Physics*, **125**, 16–56.
[28] Farge, M., 1992, Wavelet transforms and their application to turbulence. *Annual Review of Fluid Mechanics*, **24**, 395–457.
[29] Vasilyev, O.V., Yuen, D.A. and Paolucci, S., 1997, The solution of PDEs using wavelets. *Computers in Physics*, **11**(5), 429–435.
[30] Vasilyev, O.V., Podladchikov, Yu. and Yuen, D.A., 2001, Modeling of viscoelastic plume-lithosphere interaction using adaptive multilevel wavelet collocation method. *Geophysical Journal of International*, **147**(3), 579–589.
[31] Vasilyev, O. V, Podladchikov, Yu. and Yuen, D.A., 1998, Modeling of compaction driven flow in poro-viscoelastic medium using adaptive wavelet collocation method. *Geophysical Research Letters*, **25**(17), 3239–3242.
[32] Liandrat, J. and Tchamitchian, Ph., 1990, Resolution of the 1d regularized burgers equation using a spatial wavelet approximation, NASA Contractor Report 187480, ICASE Report 90-83. NASA Langley Research Center, Hampton VA 23665-5225.
[33] Kevlahan, N. and Ghidaglia, J.-M., 2001, Computation of turbulent flow past an array of cylinders using a spectral method with Brinkman penalization. *European Journal of Mechanics, B/Fluids*, **B 20**, 333–350.
[34] Vasilyev, O.V., Lund, T.S. and Moin, P., 1998, A general class of commutative filters for LES in complex geometries. *Journal of Computational Physics*, **146**, 105–123.
[35] Marsden, A.L., Vasilyev, O.V., and Moin, P., 2002, Construction of commutative filters for LES on unstructured meshes. *Journal of Computational Physics*, **175**, 584–603.
[36] Haselbacher, A. and Vasilyev, O.V., 2003, Commutative discrete filtering on unstructured grids based on least-squares techniques. *Journal of Computational Physics*, **187**(1), 197–211.
[37] Vasilyev, O.V. and Kevlahan, N.K.-R., 2005, An adaptive multilevel wavelet collocation method for elliptic problems. *Journal of Computational Physics*, **206**(2), 412–431.
[38] Guermond, J.-L. and Shen, J., 2003, Velocity-correction projection methods for incompressible flows. *SIAM Journal on Numerical Analysis*, **41**(1), 112–134.